Construction and Building Materials 116 (2016) 45–51

Contents lists available at ScienceDirect

Construction and Building Materials

journal homepage: www.elsevier.com/locate/conbuildmat

A method for the assessment of the internal structure of bio-aggregate concretes

Joseph Williams *, Mike Lawrence, Pete Walker

BRE Centre for Innovative Construction Materials, Department of Architecture and Civil Engineering, University of Bath, Bath BA2 7AY, UK

HIGHLIGHTS

- A novel method for assessing bio-aggregate composites is proposed.
- 2D and 3D image analysis used to assess aggregate orientation.
- Specimens of hemp-lime found to have a strong anisotropic internal structure.

ARTICLE INFO

Article history:
Received 20 January 2016
Received in revised form 21 April 2016
Accepted 22 April 2016

Keywords:
Bio-aggregate
Hemp-lime
Image analysis
Internal structure

ABSTRACT

The thermal and mechanical properties of bio-aggregate concretes are known to be anisotropic. This is assumed to be the result of an orientated internal arrangement of particles; the internal structure of other aggregate composite materials is known to be a determiner of physical properties and has been the focus of much study. Despite this the internal structure of bio-aggregate concretes has to date only been considered qualitatively. This work presents a novel method for the assessment of the internal structure of bio-aggregate concretes through the application of image analysis. Results are presented for the assessment of hemp-lime specimens and demonstrate a significant anisotropy within the material. These results account for anisotropic thermal and mechanical behaviour observed elsewhere and demonstrate the importance of the internal structure in determining the properties of these materials. This innovative technique represents a significant breakthrough in the search for optimisation of the performance of renewable, low carbon insulation materials. This class of materials is critical to the sustainable future of the construction industry.

1. Introduction

Bio-aggregate concretes (BAC) are formed by combining crop based aggregate, mineral binder and water. Hemp-lime, produced from the chopped up stalk (shiv) of the hemp plant, is one of the most best known but other examples include wood chips, sunflower plant stems [1] and flax plant stems [2]. As a result of the photosynthetically used carbon dioxide embodied within the plant materials, BACs have very low embodied carbon [3–5] as well as favourable thermal properties for use in building envelopes, including low thermal conductivity and high heat capacity [6–9].

To produce BACs the mixed constituents are cast into formwork or spray applied onto a substrate. Both processes apply a unidirectional compacting force to the wet material: tamping or deliberate compaction in the case of cast and force of projection in the case of sprayed. As bio-aggregate particles are often elongated in form, this compacting force is considered by most to have significant influence on their arrangement, the elongated particles tending towards stratified planes that are perpendicular to compacting force [10,11].

The anisotropic arrangement concept is supported by observations of some physical properties. Nguyen [12] measured the thermal conductivity of cast-compressed hemp-lime specimens both parallel and perpendicular to the compacting force and found up to a 30% higher thermal conductivity in the perpendicular direction. Other work has reported similar findings for cast-tamped material [13] and sprayed material [14]. In all cases the observations were attributed to the internal structure, in which the stratified planes are opposing the transverse heat transfer.

The compressive behaviour of BACs has also been studied with respect to orientation of the bio-aggregates. Previous studies have observed that the peak compressive strength of these materials is higher when loaded parallel to the compacting force however the

* Corresponding author.
E-mail address: J.P.Williams@bath.ac.uk (J. Williams).

http://dx.doi.org/10.1016/j.conbuildmat.2016.04.088
0950-0618/

Nomenclature

Symbols

x_i, y_i, z_i	the location of a given pixels/voxels within any given shape comprising n connected pixels/voxels
m_{pqr}	the global image moments of a given shape comprising n connected pixels/voxels
u_{pqr}	the central image moments of a given shape comprising n connected pixels/voxels
$\bar{x}, \bar{y}, \bar{z}$	the location of the centroid of any given shape comprising n connected pixels/voxels
$\theta_{xy}, \theta_{yz}, \theta_{zx}$	the orientation of the principle axis of the best fit ellipse for any given shape comprising n connected pixels/voxels
f	the frequency of particles observed at a given orientation
n	experimentally derived constant

compressive stiffness is lower [15–17]. Additionally the material has been observed to fail in a more brittle manner when loaded perpendicularly. Fig. 1 shows the average compressive stress/strain plots of three 150 mm cube specimens of hemp lime and highlights this difference in behaviour that can be attributed to the internal structure – the strata providing differing transverse and parallel load paths.

Studies of other particulate composite materials such as asphalt [18,19] and soil [20], have demonstrated that the arrangement of the internal structure in these cases is one of the contributing factors for the global properties and a cause of anisotropic behaviour. Despite this, and the observation of anisotropic properties, there has, to the authors' knowledge, been no attempt to measure the internal structure of bio-aggregate concretes, for orientation or for any other parameter.

In order to test the hypothesis of compaction generating strata within bio-aggregate concretes, this paper outlines an image analysis method for the statistical assessment of particle orientation within cast material. The method is based on established methods for other materials as well as image analysis methods already in use for the study of the size distribution of bio-aggregate particles. Results are reported from the application of this method to three variants of the bio-aggregate concrete hemp-lime.

2. Methodology

2.1. Materials and specimen production

All the specimens considered in this work were produced using hemp shiv grown in the UK the properties of which are presented in Table 1. The particle size distribution of bio-aggregates length and width can be determined by two dimensional digital image analysis as established by others [21]. A 20 g sample of shiv was assessed in this way with the results presented in Fig. 2. The results presented in Table 1 and Fig. 2 indicate that the material used in this study is comparable to that used widely elsewhere in the literature and that the shiv particles can be considered to be of elongated form.

The binder used was pre-formulated for hemp-lime construction. The specific formulation of the binder is not declared by the manufacturer, however it is believed to be mainly hydrated lime with additional pozzolanic additives and cement.

To produce the composite material the constituents were mixed in a revolving pan mixer by first slaking the binder with the water and then adding the hemp and further mixing until uniformly combined. For each specimen a set mass of material was tamped into a 150 mm cube mould fitted with a collar to allow for initial overfilling. Three variations of material, standard, light weight and compact, were used in the study Table 2. The standard mix represents an industry standard hemp-lime formulation for walling applications. The light weight mix represent a material with the same proportion of hemp per unit volume but a lower binder content; the compacted mix represents a higher density version of the standard mix but with the same binder to aggregate ratio.

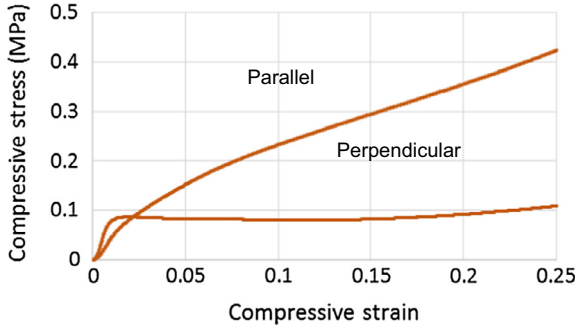

Fig. 1. Stress strain plots for perpendicular and parallel loaded hemp-lime cubes produced with a ratio of 16% hemp, 36% binder and 48% water and cast in three layers of 0.66 kg with vertical compaction applied between each layer.

2.2. Image analysis

Image analysis is the process of imaging a material either in two or three dimensions and then using analysis conducted on the image to extract meaningful data. In this application the required outcome was to gauge if a preference of orientation is present in the particles of the material and the process utilised was as follows:

Table 1
Properties of hemp shiv.

Bulk density (kg m^{-3})	Particle length (mm)		Particle width (mm)	
	Mean particle length (mm)	Standard deviation	Mean	Standard deviation
108	5.56	5.49	1.55	1.33

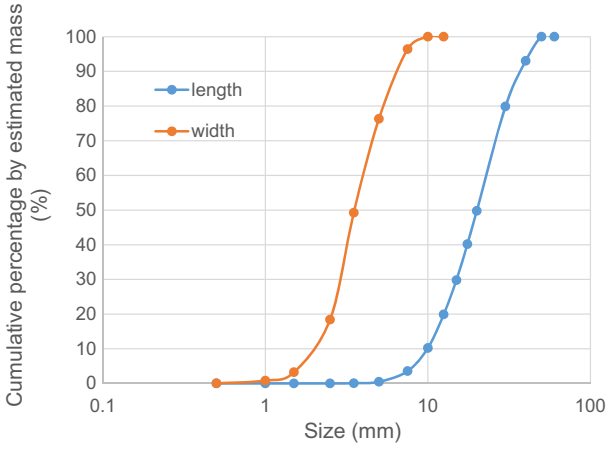

Fig. 2. Particle size distribution of hemp shiv as obtained by two dimensional image analysis of a 20 g sample.

Table 2
Hemp-lime mixture variations.

Mixture	Aggregate (bulk%)		Binder (bulk%)		Water (bulk%)		Paste (%)		Wet mass of specimen (kg)	Estimated Porosity (Fresh state%)	Average dry density (kgm^{-3})
	Mass	Vol	Mass	Vol	Mass	Vol	Mass	Vol			
Standard	16	56	36	23	48	21	84	32	2.00	66	284
Light weight	21	64	36	20	43	16	79	25	1.48	84	353
Compacted	16	56	36	23	48	21	84	32	2.41	60	422

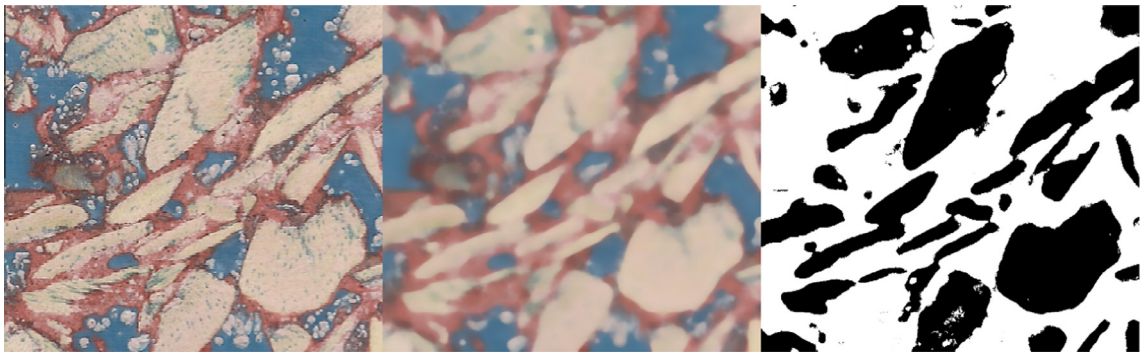

Fig. 3. Left to right: original VD image, image passed through median filter, image passed through threshold filter.

Table 3
Image enhancement and filtering settings trialled, those deemed most appropriate identified in bold.

Process	ImageJ settings	Avizo® Fire 8 settings
Median filter	Radius (pixels): 5, 10, 15, **20**, 25, 30	Iterations: 5, **6**, 7
Colour threshold lower boundary	8 bit hue value: 10, 12, **14**, 16, 18, 20	32 bit float intensity value: **4**, 5, 6 (basic mix) 4, 4.5, **5** (light mix) 6, **7**, 8 (compacted mix)
Colour threshold upper boundary	8 bit hue value: **50**	32 bit float intensity value: 28, **29**, 30 (basic mix) 8, 8.5, **9** (light mix) 28, **29**, 30 (compacted mix)
Opening algorithm	Iterations: 1, 2, **3**, 5, 10, 15, 20, 25	Radius (voxels) 1, 2, **3**

- image the material;
- segregate out the shiv;
- identify and measure the orientation of the particles;
- perform a frequency analysis of the population.

Similar methods, but for the study of other materials, have already been developed and were used as a reference for application to bio-aggregate concretes. These include asphalt [22,23], soil [20], fibre reinforced concrete [24,25] and fibre board [26,27]. Image analysis has also been applied to investigate the size distribution of bio-aggregate particles [21] and was used as an additional reference. Two methods of imaging were considered within the study in order to provide comparison and validate results: visual digital imaging (VD imaging) and computer tomography scanning (CT scanning).

VD imaging is conducted by taking physical sections of the material and imaging the exposed face using a digital camera or flat-bed scanner. An advantage of this method is its low cost however it is a destructive method and requires imaging in several orientations in order to assess the three dimensional topology. Further disadvantages specific to use with BACs are the similar colouring of the particles and binder and the large number of voids that makes visual differentiation of components difficult.

In this study, pairs of specimens were VD imaged, one parallel to compacting force and one perpendicular. Each specimen was sectioned into six 150 mm square slices using a band saw. To improve the visual contrast between material and voids, the slices were submerged in a low viscosity coloured resin. Once cured, the faces were sanded to remove excess and scanned with a flatbed scanner at a resolution of 2400 dpi. To improve contrast between the binder and the hemp, a coloured pigment was added to the binder during the specimen production at a dose of 10 g per specimen.

CT scanning is an established method of imaging the internal structure of materials producing a map of the X-ray absorbance within the material, a property closely linked to density. Advantages of this method are that it is non-destructive and produces a three dimensional image of the material. It is however expensive in comparison to VD imaging and the contrast within the parameters it measures cannot be enhanced by physical pre-treatments.

Within this study all CT scans were taken using a Nikon XTEK, XTH 225 ST CT scanner set to 165 kV and 165 μA. The data were recompiled into a three dimensional volume using Avizo® Fire 8.

2.3. Segregation

To identify the shiv within the images, two image filters with successful precedents for other materials [23,28,29] were applied: a median filter and a threshold filter. The same processes were implemented for both two dimensional and three dimensional images, however differing programs and settings were used due to the differing image formats. ImageJ and Avizo® Fire 8 were used for the two dimensional and three dimensional images respectively.

A median filter replaces each two dimensional pixel's, or three dimensional voxel's, value with the median of those within a specified radius [30,31]. This has the result of smoothing the image and removing anomalies Fig. 3. A threshold filter is used to segregate the smoothed image. Each pixel/voxel is in turn assessed against a set of criteria in order to produce a binary image [30,31]. Careful selection of the criteria enables the identification of a single component and in this case was used to identify the shiv Fig. 3.

Both the median filter and threshold filter applied by each program are controlled by operator assigned settings. The nature of these settings differs between the two programs used, however, in both cases their selection will have a bearing on the analysis results. To assess the sensitivity of the analysis to the choice of settings used, a sensitivity analysis was undertaken on a single image from each imaging method. The range of settings considered for each of the imaging methods is presented in Table 3.

2.4. Identification and measuring orientation

Within the binary images, particles are considered to be regions of interconnected positive pixel/voxels. Due to the close proximity of particles and the limited resolution of the images, there are regions where several aggregates may be

Fig. 4. Left to right: thresholded image, image passed through opening algorithm, image assessed for particles and represented as best fitting ellipses.

misinterpreted as a single particle due to touching areas. To help mitigate the extent of misinterpreted particle groups, an opening algorithm was applied to the images prior to final assessment Fig. 4.

Opening algorithms selectively remove and then add additional positive pixels or voxels based on the values of those around it [30,31]. These are commonly used at this stage of image analysis in order to clean the images and help remove bridges between adjoining particles. As the opening algorithm in both cases was controlled by a user assigned setting, again a range of settings was trialled with details given in Table 3.

To measure the orientation of the identified particles, inbuilt tools within the respective programs were used. The process in both cases is based on calculation and interpretation of the first and second order image moments and is detailed fully elsewhere [32,33]. For each group of n connected pixels/voxels, the global first and second moments are calculated:

$$m_{pqr} = \sum_{i=1}^{n} x_i^p y_i^q z_i^r \tag{1}$$

The central second moments: u_{200}, u_{020}, u_{002}, u_{011}, u_{101}, and u_{110} and the centroid coordinates can then be determined:

$$u_{pqr} = m_{pqr} - \frac{m_{100}^p m_{010}^q m_{001}^r}{m_{000}} \tag{2}$$

$$\bar{x} = \frac{m_{100}}{m_{000}} \tag{3}$$

$$\bar{y} = \frac{m_{010}}{m_{000}} \tag{4}$$

$$\bar{z} = \frac{m_{001}}{m_{000}} \tag{5}$$

By equalising the second moments and centroid of the particle with that of an ellipse or ellipsoid, the best fitting ellipse or ellipsoid can be determined Fig. 4. This enables a consistent measurement of geometrical properties of particles despite their irregular shapes. The orientation of the principal axis of the ellipse or ellipsoid was used as the measure of particle orientation and can be found in each 2D plane:

$$\theta_{xy} = \frac{1}{2}\tan^{-1}\left(\frac{2u_{110}}{u_{200}u_{020}}\right) \tag{6}$$

$$\theta_{yz} = \frac{1}{2}\tan^{-1}\left(\frac{2u_{011}}{u_{020}u_{002}}\right) \tag{7}$$

$$\theta_{zx} = \frac{1}{2}\tan^{-1}\left(\frac{2u_{101}}{u_{002}u_{200}}\right) \tag{8}$$

2.5. Frequency analysis

For visual digital imaging, twelve images were produced for each mix: six taken parallel to compaction and six perpendicular. For each mix a cumulative frequency distribution was produced in each direction for the total particle population from all six slices. In the case of CT scanning, one image was taken per mix with two values of particle orientation measured that equate to the same parallel and perpendicular viewpoints. For each mix a cumulative frequency distribution was produced in each direction for the total particle population of the image. In both cases only particles above a minimum size of 1 mm^2 and 1 mm^3 respectively were considered. The data from both imaging methods were manipulated to give an orientation scale of between 0° and 90° which represent horizontal and vertical alignment in the image plane respectively.

3. Results

3.1. Sensitivity to image enhancement parameters

The perpendicular frequency distributions obtained from one image but using the range of parameters provided in Table 3 were compared. In each instance a version of the Hankinson equation [34], Eq. (9), was fitted to the distribution using a least squares approach and the determined values of f_0, f_{90} and n used as indicators by which to compare the distributions. Hankinson's equation was originally developed for modelling the compressive stress of spruce with respects to orientation of the grain but has since been developed for modelling other properties of timber as well as wood based particle composite boards [35–37]. Hankinson's equation was selected due to strong similarities between distribution forms observed in this study and those where the equation has been previously applied. In addition the boundary criteria, f_0 and f_{90}, enable the distribution to be applied both to the 2D images, where a lower bound frequency can be observed, as well as the 3D images. To the author's knowledge Hankinson's equation has not previously been used to model frequency of orientated particles/fibres however the

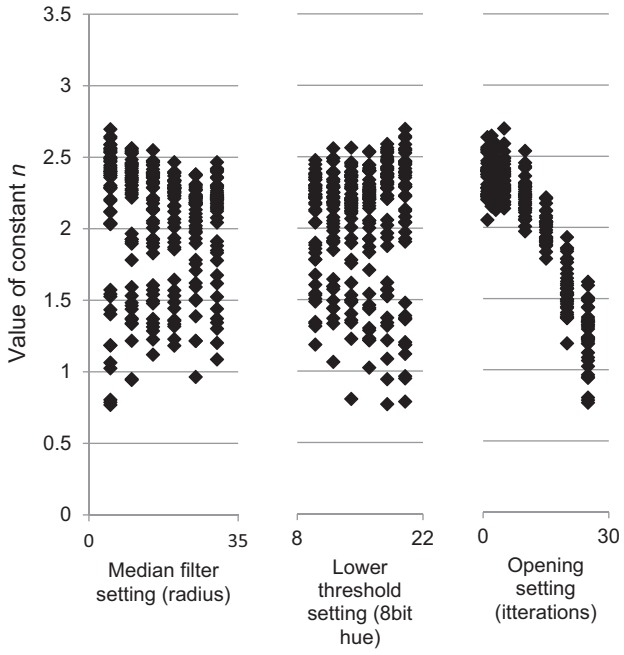

Fig. 5. The value of the constant n obtained using differing enhancement setting with 2D images.

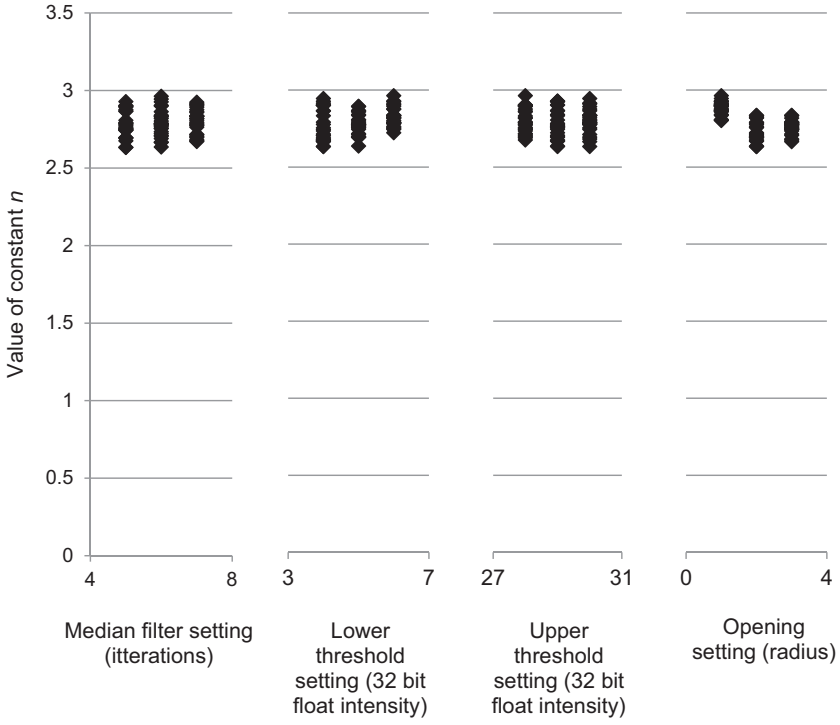

Fig. 6. The value of the constant n obtained using differing enhancement setting with 3D images.

wrapped Cauchy distribution that can be manipulated into the same "Hankinson" form has been used successfully [38].

$$f = \frac{f_0 f_{90}}{f_0 \sin^n \theta + f_{90} \cos^n \theta} \tag{9}$$

The values of n, for differing enhancement parameters, are presented for the standard mix in Figs. 5 and 6. for two dimensional and three dimensional images respectively. The values of f_0 and f_{90} with respect to the enhancement parameters, while not shown, exhibit similar patterns and the same pattern was found in all three mix designs.

In Figs. 5 and 6 it is evident that the enhancement parameters can have a significant influence on the value of n and therefore the distribution produced; for the visual digital imaging method it was determined that the range of parameters considered was able to effect a 10% variation in the peak frequency of the distribution. The opening algorithm can be seen to be the most onerous process and the smaller number of opening algorithm variations considered in the CT data is the likely reason for the smaller spread of results in this case. When the opening algorithm iterations are restricted to under three iterations for the digital visual image data, the variation in peak frequencies is reduced to 2.4% and is comparable to the variation in the CT images.

In order to select appropriate parameters to use for the full assessment, the enhanced images from the sensitivity study were compared against the original images by eye. This was conducted using a "winner stays on" system whereby two images were compared to the original with the one judged least effective at identifying hemp particles being replaced. The process was continued until all permutations had been considered. The parameters identified as most appropriate by this method are identified in Table 3.

3.2. Particle orientation frequency analysis

The particle orientation frequency distributions from VD imaging using the enhancement and filtering setting identified in Table 3 are presented in Fig. 7. The resulting distributions, viewing both perpendicularly and parallel to the direction of compacting

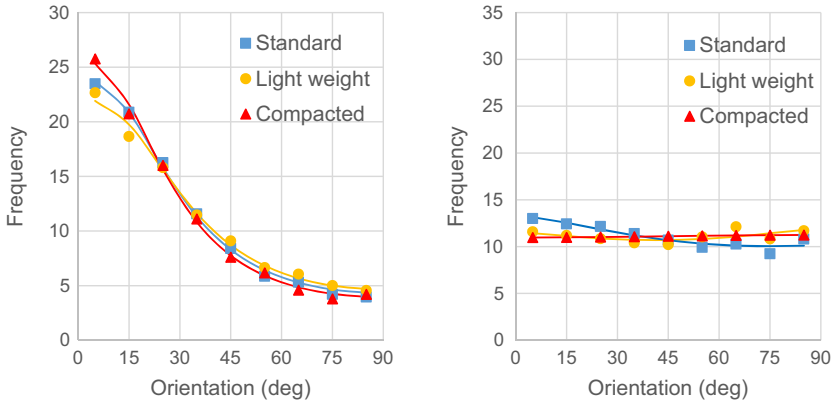

Fig. 7. Frequency distribution of particle orientation produced using two dimensional imaging. Perspective perpendicular to compaction, left, and parallel to compaction, right.

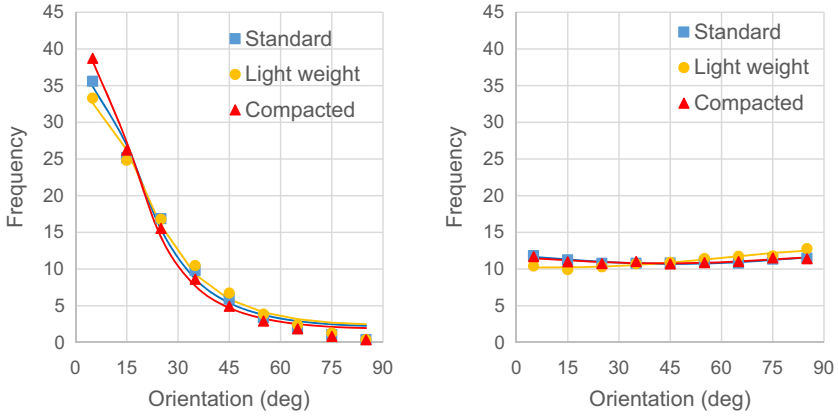

Fig. 8. Frequency distribution of particle orientation produced using CT imaging. Perspective perpendicular to compaction, left, and parallel to compaction, right.

force, are shown as are the distributions produced from all three mixes. Eq. (9) has been fitted to the data in using a least squares approach each case to aid comparison. The equivalent distributions produced using CT imaging are presented in Fig. 8.

4. Discussion

4.1. Comparison of material in opposing directions

From Figs. 7 and 8 it can be seen that the frequency distribution of particle orientations viewed parallel to compacting force is flat: indicative of a random distribution and suggests the structure is isotropic in this plane. Conversely, in the perpendicular plane, the frequency distribution of particle orientations is strongly swayed. This indicates a preference of orientation within the population and is therefore suggestive that the material's structure is anisotropic in this plane.

The finding of both an anisotropic and isotropic distributions in contrasting directions is supportive of the hypothesis that compaction force produces a preferential orientation [10,12]. A clear tendency is observed in all specimens for the major axis of the particles to tend towards horizontal planes, perpendicular to the compaction force. This observation concurs with, and provides an explanation for the observations of others that several physical properties of bio-aggregate composites exhibit anisotropic behaviour with respect to the direction of compaction force [15–17].

4.2. Comparison of materials produced using differing formation variables

In the perpendicular perspective, a consistent difference between distributions produced from the differing mixes is present in the results from both methods. The light mix is observed to have the lowest maximum frequency and highest minimum frequency; the compacted mix is observed to have the highest maximum frequency and lowest minimum frequency.

A possible interpretation is that the overall degree of orientation is higher in the compacted material and lower in the low density material compared to the standard mix. This is logical in the case of the compacted mix where the ratio of constituents was the same but level of compaction was known to be higher. For the light weight mix, the density of hemp in the material was controlled to be the same as the standard mix and this was assumed to indicate a similar compaction level and thus the cause of the apparently lower degree of orientation in the case of the lightweight mix can therefore not be attributed to compaction. Alternately it is proposed that the aggregate volume fraction may be a determining factor in the degree of orientation; a lower volume of aggregates producing a higher level of inter-particle porosity and increasing the ability of particles to rotate under compaction. It is considered likely therefore that both compaction and aggregate volume fraction will impact the degree of orientation and further experiments to investigate the impact of both variables on the internal structure are proposed.

The observed difference between the frequency distributions from the three mixes is noted to fall within the difference obtained using differing image enhancement settings and highlights the importance of using consistent settings for comparing material. A consistent set of enhancement settings was used across all specimens analysed with VD imaging and so removes this as a source of uncertainty in this case. The variation observed in the perpendicular perspective was also noted to be of greater magnitude than those observed in the parallel perspective. This indicates that the observations in the perpendicular perspective are within the natural variation of the population and therefore the observation that there are differing degrees of orientation, while promising, is statistically insignificant and undermines any firm conclusions at this stage.

4.3. Comparison of digitisation methods

The frequency distributions produced by the VD imaging Fig. 7, are observed to be of the same general form of those produced using CT images Fig. 8. In each case the parallel perspective has produced a relatively level distribution with all frequencies approximately between 9% and 14%. In the perpendicular perspective both methods have indicated a swayed distribution towards the horizontal with a similar form in both cases. In both cases the ordering of the mixes, least to most orientated, is the same. A smoother frequency distribution was found using the CT images as opposed to the VD imaging and is attributed to the larger overall population of particles measured.

In the perpendicular view, the CT generated images have, in all variations of material, yielded distributions with a consistently higher frequency range. This difference is attributed to the differing nature of the methods; VD imaging analysis measures a random section through each particle while CT scan analysis measures the whole particle and indicates that a consistent method must be adopted for the comparison of material.

The strong correlation between the results from both methods provides a high level of confidence in the results. VD imaging conducted in two planes is considered sufficient to infer the three dimensional structure of the material and, due to the lower costs,

is considered to be the more practical of the two methods for larger samples of material.

5. Conclusion

In this work the novel application of image analysis methodology for the assessment of the internal structure of bio-aggregate concretes was trialled. It was shown that similar results are obtainable using two differing methods of imaging: CT scanning and VD imaging. This indicates that both procedures are capable of producing reliably analysable images and that image analysis is a suitable method for the assessment of these materials.

The results in this study support the established theory that these materials have an orientated internal structure that is determined by the direction of any compacting force. A consistent difference was also observed between materials constructed in differing ways and, while this was within the natural variation of the results, indicates that the production method is likely to determine the degree of orientation.

This study demonstrates that image analysis is a reliable and repeatable method of assessing the internal structure of bio-aggregate concretes. This will facilitate the development of models which will better predict the impact of construction processes on the mechanical and hygrothermal properties of these materials, leading to the potential optimisation of their performance. Additional work is required to establish the exact way in which construction processes influence the internal structure of bio-aggregate concretes in order to utilise this aspect of the material.

Acknowledgements

The authors gratefully acknowledge the financial support provided by the Engineering and Physical Sciences Research Council – United Kingdom, EP/L016869/1.

References

[1] V. Nozahic, S. Amziane, G. Torrent, K. Saïdi, H. De Baynast, Design of green concrete made of plant-derived aggregates and a pumice–lime binder, Cement Concr. Compos. 34 (2) (2012) 231–241.
[2] A. Korjenic, V. Petránek, J. Zach, J. Hroudová, Development and performance evaluation of natural thermal-insulation materials composed of renewable resources, Energy Build. 43 (9) (2011) 2518–2523.
[3] M. Boutin, C. Flamin, S. Quinton, G. Gosse, Analyse du Cycle de Vie de Mur en Béton Chanvre Banché sur Ossature en Bois, INRA, Lille, France, 2005.
[4] K. Ip, A. Miller, Life cycle greenhouse gas emissions of hemp–lime wall constructions in the UK, Resour. Conserv. Recycl. 69 (2012) 1–9.
[5] S. Pretot, F. Collet, C. Garnier, Life cycle assessment of a hemp concrete wall: Impact of thickness and coating, Build. Environ. 72 (2014) 223–231.
[6] L. Arnaud, D. Samri, É. Gourlay, Hygrothermal Behavior of Hempcrete. Bio-aggregate-based Building Materials, John Wiley & Sons, 2013, pp. 179–242.
[7] F. Collet, S. Pretot, Experimental highlight of hygrothermal phenomena in hemp concrete wall, Build. Environ. 82 (2014) 459–466.
[8] M. Lawrence, E. Fodde, K. Paine, P. Walker, Hygrothermal performance of an experimental hemp-lime building, Key Eng. Mater. 517 (2012) 413–421.
[9] F. Collet, S. Prétot, Thermal conductivity of hemp concretes: variation with formulation, density and water content, Constr. Build. Mater. 65 (2014) 612–619.
[10] Y. Hustache, L. Arnaud, Synthèse des connaissances sur les bétons et mortiers de chanvre, Construire en Chanvre, 2008.
[11] S. Elfordy, F. Lucas, F. Tancret, Y. Scudeller, L. Goudet, Mechanical and thermal properties of lime and hemp concrete ("hempcrete") manufactured by a projection process, Constr. Build. Mater. 22 (10) (2008) 2116–2123.
[12] T.T. Nguyen, V. Picandet, P. Carre, T. Lecompte, S. Amziane, C. Baley, Effect of compaction on mechanical and thermal properties of hemp concrete, Eur. J. Environ. Civ. Eng. 14 (5) (2010) 545–560.
[13] T. Dinh, C. Magniont, M. Coutand, G. Escadeillas, Hemp concrete using innovative pozzolanic binder, in: First International Conference on Bio-based Building Materials, 2015. Clermont-Ferrand, France.
[14] T. Pierre, T. Colinart, P. Glouannec, Measurement of thermal properties of biosourced building materials, Int. J. Thermophys. 35 (9–10) (2014) 1832–1852.
[15] S. Amziane, V. Nozahic, M. Sonebi, Design of mechanically enhanced concrete using hemp shiv, in: First International Conference on Bio-based Building Materials, 2015. Clermont-Ferrand, France.
[16] A. Kashtanjeva, M. Sonebi, S. Amziane, Investigation of the mechanical performance and drying shrinkage of hemp concrete, in: First International Conference of Bio-based Building Materials Clermont-ferrand, France, 2015.
[17] A. Youssef, T. Lecompte, V. Picandet, N. Challamel, Compressive and shearing behaviour of lime and hemp concrete, in: First International Conference on Bio-based Building Materials, 2015. Clermont-Ferrand, France.
[18] M. Hamzah, W. Von, N. Abdullah, Effects of compactor types on aggregate orientation of asphalt mixtures, Int. J. Eng. Trans. A Basics 26 (7) (2013) 677.
[19] E. Sanchez-Alonso, A. Vega-Zamanillo, D. Castro-Fresno, Effect of type of compaction on mechanical properties in warm-mix asphalts, J. Mater. Civ. Eng. 24 (8) (2012) 1043–1049.
[20] B. Shi, Y. Murakami, Z. Wu, Orientation of aggregates of fine-grained soil: quantification and application, Eng. Geol. 50 (1) (1998) 59–70.
[21] V. Picandet, Characterization of Plant-Based Aggregates. Bio-aggregate-based Building Materials, John Wiley & Sons, 2013, pp. 27–74.
[22] M.E. Kutay, E. Arambula, N. Gibson, J. Youtcheff, Three-dimensional image processing methods to identify and characterise aggregates in compacted asphalt mixtures, Int. J. Pavement Eng. 11 (6) (2010) 511–528.
[23] N. Roohi Sefidmazgi, H.U. Bahia, Effect of compaction conditions on aggregate packing using 2-dimensional image analysis and the relation to performance of HMA, Mater. Struct. 47 (8) (2014) 1313–1324.
[24] Y. Akkaya, S. Shah, B. Ankenman, Effect of fiber dispersion on multiple cracking of cement composites, J. Eng. Mech. 127 (4) (2001) 311–316.
[25] J. Liu, C. Li, J. Liu, G. Cui, Z. Yang, Study on 3D spatial distribution of steel fibers in fiber reinforced cementitious composites through micro-CT technique, Constr. Build. Mater. 48 (2013) 656–661.
[26] E. Badel, C. Delisee, J. Lux, 3D structural characterisation, deformation measurements and assessment of low-density wood fibreboard under compression: the use of X-ray microtomography, Compos. Sci. Technol. 68 (7–8) (2008) 1654–1663.
[27] G. Standfest, S. Kranzer, A. Petutschnigg, M. Dunky, Determination of the microstructure of an adhesive-bonded medium density fiberboard (MDF) using 3-D sub-micrometer computer tomography, J. Adhes. Sci. Technol. 24 (8–10) (2010) 1501–1514.
[28] I. Bessa, V. Castelo Branco, J. Soares, Evaluation of different digital image processing software for aggregates and hot mix asphalt characterizations, Constr. Build. Mater. 37 (2012) 370–378.
[29] A.R. Coenen, M.E. Kutay, N.R. Sefidmazgi, H.U. Bahia, Aggregate structure characterisation of asphalt mixtures using two-dimensional image analysis, Road Mater. Pav. Design 13 (3) (2012) 433–454.
[30] FEI Visualization Sciences Group, Avizo 8, Avizo User's Guide, English, Konrad-Zuse-Zentrum für Informationstechnik, Berlin, Germanry, 2014.
[31] T. Ferreira, W. Rasb, ImageJ user guide, 2012.
[32] H. Ming-Kuei, Visual pattern recognition by moment invariants, IRE Trans. Inform. Theory 8 (2) (1962) 179–187.
[33] M.R. Teague, Image analysis via the general theory of moments*, J. Opt. Soc. Am. 70 (8) (1980) 920–930.
[34] R. Hankinson, Investigation of crushing strength of spruce at varying angles of grain, Air Serv. Inform. Circ. 3 (259) (1921) 130.
[35] H. Holmberg, Influence of grain angle on Brinell hardness of Scots pine *(Pinus sylvestris L.)*, Holz als Roh- und Werkstoff 58 (1) (2000) 91–95.
[36] S. Kazemi Najafi, A. Abbasi Marasht, G. Ebrahimi, Prediction of ultrasonic wave velocity in particleboard and fiberboard, J. Mater. Sci. 42 (3) (2007) 789–793.
[37] T. Nishimura, P.M. Ansell, Monitoring fiber orientation in OSB during production using filtered image analysis, Wood Sci. Technol. 36 (3) (2002) 229–239.
[38] K. Schulgasser, Fibre orientation in machine-made paper, J. Mater. Sci. 20 (3) (1985) 859–866.